

Gaussian and non-Gaussian speckle fluctuations in the diffusing-wave spectroscopy signal of a coarsening foam

A.S. Gittings¹ and D.J. Durian^{1,2}

¹*University of California, Department of Physics & Astronomy, Los Angeles, CA 90095*

²*University of Pennsylvania, Department of Physics & Astronomy, Philadelphia, PA 19104*

djdurian@physics.upenn.edu

All prior applications of Diffusing-Wave Spectroscopy (DWS) to aqueous foams rely upon the assumption that the electric field of the detected light is a Gaussian random variable and that, hence, the Siegert relation applies. Here we test this crucial assumption by simultaneous measurement of both second and third-order temporal intensity correlations. We find that the electric field is Gaussian for typical experimental geometries equivalent to illumination and detection with a plane wave, both for backscattering and transmission through an optically-thick slab. However, we find that the Gaussian character breaks down for point-in / point-out backscattering geometries in which the illumination spot size is not sufficiently large in comparison with the size of the intermittent rearrangement events. © 2018 Optical Society of America

OCIS codes: 290.7050 Turbid media; 300.6480 Spectroscopy, speckle; 999.9999 Photon correlation spectroscopy.

submitted to *Applied Optics* as a Photon Correlation and Scattering feature paper

1. Introduction

Aqueous foams consist of a dispersion of gas within a surfactant stabilized liquid network.¹⁻⁴ Foams have many practical uses including fire fighting agents, food and beverage products, and oil recovery. Their structure is meta-stable, constantly evolving by gas diffusion, bubble rearrangement, drainage, and bubble rupture. In fact, if one waits long enough, the end result for a foam is always the same: one gas bubble with no intervening liquid. Foam rheology is robust, displaying both solid and liquid behavior for small and large shear stress, respectively. In addition, foams present an experimentally accessible example of a jammed system, an important class of systems for which the physics is still not fully understood.

Visible light entering a foam is easily scattered due to the index of refraction mismatch at the liquid and air interfaces. Naturally occurring foams are disordered, producing randomly oriented scattering sites. As such, photons perform an effective random walk as they scatter through the foam.⁵⁻⁹ This multiple scattering of light gives foams their white appearance and renders more traditional observation techniques, such as video imaging, ineffectual for examining foam structure in the bulk.

Diffusing-wave spectroscopy (DWS) is a general method for taking advantage of multiple light scattering for a non-invasive probe of the dynamics of the scattering sites.¹⁰⁻¹² As in the more usual single-scattering photon-correlation technique,¹³⁻¹⁵ the time trace of the intensity $I(t) = E(t)E^*(t)$ of roughly one speckle of scattered light is measured, and the intensity autocorrelation is computed:

$$g^{(2)}(\tau) = \langle I(0)I(\tau) \rangle / \langle I \rangle^2. \quad (1)$$

If the statistics of the underlying electric field are Gaussian, then the right hand side of this equation is a four-time electric field correlation that can be expressed as the sum of products of two-time field correlations. The result simplifies to the well-known Siegert relation,

$$\begin{aligned} g^{(2)}(\tau) &= 1 + \beta \frac{|\langle E(0)E^*(\tau) \rangle|^2}{|\langle EE^* \rangle|^2} \\ &= 1 + \beta |\gamma(\tau)|^2, \end{aligned} \quad (2)$$

where β is a constant that depends on the ratio of speckle to detector size.¹³⁻¹⁵ The Siegert relation is crucial since it relates the experimentally-measured intensity fluctuations to the normalized electric field autocorrelation function, $\gamma(\tau)$, from which the scattering site dynamics can be determined.

The above procedure has been used in DWS studies of bubble rearrangements in aqueous foams under several different circumstances. For coarsening foams, the diffusion of gas from smaller to larger bubbles causes sudden stick/slip-like rearrangement of several neighboring bubbles at a time.¹⁶⁻¹⁸ For foams subjected to steady shear, the macroscopic deformation is accomplished by microscopic bubble-scale rearrangements.^{19,20} After cessation of shear, coarsening-induced rearrangements are suppressed until the bubble-size distribution noticeably changes by further coarsening.^{20,21} For oscillating shear, the size of echoes in the DWS signal can be used as a measure of microscopic reversibility in the bubble motion.^{22,23}

The Siegert relation requires an assumption that the electric field $E(t)$ be a Gaussian variable of zero mean. Though this condition is satisfied for many experimental situations, it can break down if the scattering sites are few in number, correlated, or if the dynamics systematically change with time. In addition, some experimental pitfalls, such as limited laser coherence, or a static component in the scattered field, can lead to failure. None of these possibilities can be eliminated by inspection of $g^{(2)}(\tau)$ alone.

Higher-order statistics can be measured to verify whether or not the Siegert relation can be invoked to extract the electric field autocorrelation from the measured intensity autocorrelation.^{24–26} This only involves further processing of the same bitstream of photon counts. No additional auxiliary optical setup is needed, as in heterodyning. In this paper, we measure the three-time intensity correlation, simultaneously with $g^{(2)}(\tau)$, for coarsening foams to determine if the electric field fluctuations are indeed Gaussian, as assumed in prior studies. We begin by describing our experimental methods and applying them to a controlled sample of diffusing polystyrene spheres, known in advance to possess Gaussian field fluctuations. After thus verifying our apparatus and procedures, we investigate the nature of the electric field fluctuations for light scattered from a coarsening foam.

2. Optical Methods

A typical experimental setup for DWS consists of a coherent laser, the sample, a photon counting device, and a digital correlator. We use a Coherent Verdi-V5 (5W) diode-pumped solid-state laser operating at $\lambda = 532nm$. Scattered light is collected into a photodetector using a single mode optical fiber with GRIN lens and line filter. The analog photocurrent signal is then amplified and discriminated such that each photon produces a TTL logic pulse. For a typical DWS measurement, the resulting bitstream $n(t)$ is sent to a commercial correlator (Flexible Instruments FLEX1000) for our experiment, which computes the autocorrelation of the bitstream:

$$g^{(2)}(\tau) = \langle n(0)n(\tau) \rangle / \langle n \rangle^2. \quad (3)$$

The right hand side of this equation represents the photon-count autocorrelation function; $n(t)$ is the number of photons detected between times t and $t + \tau_s$, where τ_s is the sampling time. This is equivalent to the intensity autocorrelation function.

Next, we set out to measure time slices of fixed T of the third order intensity correlation function:

$$g^{(3)}(\tau, \tau + T) = \frac{\langle I(0)I(\tau)I(\tau + T) \rangle}{\langle I \rangle^3}. \quad (4)$$

We supplement the usual DWS set-up, described above, with a custom-built synchronizing multiplying digital delay line SMDDL. The same hardware and procedure from our earlier work was employed.^{24–26} The delay line takes the un-synchronized TTL bitstream, $n_u(t)$, and outputs two synchronized bitstreams: $n_A(t) = n(t)$; and $n_B(t) = n(t)n(t + T)$. The delay time, T , can be set from 50 ns to about 50 ms in increments of 50 ns. The two synchronized bitstreams $n_A(t)$ and $n_B(t)$ are fed to the digital correlator as inputs. Auto-correlating channel A produces $g^{(2)}(\tau)$ given by Eq. (3). The cross-correlation of channel A and B , $\langle n_A(0)n_B(\tau) \rangle / (\langle n_A \rangle \langle n_B \rangle)$, produces a slice of the three-time correlation:

$$\hat{g}^{(3)}(\tau, \tau + T) = \frac{\langle n(0)n(\tau)n(\tau + T) \rangle}{\langle n_A \rangle \langle n_B \rangle}, \quad (5)$$

where T and τ are the delays introduced by the SMDDL and the correlator, respectively, and $\langle n_A \rangle$ and $\langle n_B \rangle$ are the average number of counts per sampling time for channels A and B . The raw correlation $\hat{g}^{(3)}(\tau, \tau + T)$ does not have the correct normalization for comparison with $g^{(3)}(\tau, \tau + T)$. This can be recovered by noting that $\langle n_A \rangle = \langle n \rangle = R_A \tau_s$ and $\langle n_B \rangle = \langle n(\tau)n(\tau + T) \rangle = R_B \tau_s$, where R_A and R_B are the count rates measured by correlator channels A and B , respectively. Properly normalized, we have

$$g^{(3)}(\tau, \tau + T) = \frac{\langle n_B \rangle}{\langle n_A \rangle^2} \hat{g}^{(3)}(\tau, \tau + T) = \frac{\langle n(0)n(\tau)n(\tau + T) \rangle}{\langle n \rangle^3}, \quad (6)$$

$$= \frac{R_B}{\tau_s R_A^2} \hat{g}^{(3)}(\tau, \tau + T). \quad (7)$$

The three-time counts correlation function, given by the right hand side of Eq.(6), is equivalent to the three-time intensity correlation function Eq.(4) since each photon count produces a digital TTL pulse. The right hand side of Eq.(7) represents the experimental measurement of $g^{(3)}(\tau, \tau + T)$. Altogether, we are thus able to measure both $g^{(2)}(\tau)$ and a constant- T slice of $g^{(3)}(\tau, \tau + T)$ simultaneously.

Next, we generate the three-time Gaussian prediction $g_G^{(3)}(\tau, \tau + T)$. The first step is to extract $\gamma(\tau)$ and $\beta = \langle I^2 \rangle / \langle I \rangle^2 - 1$ from $g^{(2)}(\tau)$, assuming that the Siegert relation Eq.(2) is valid. For Gaussian scattering processes, intensity correlation functions of any order can be expressed in terms of sums of products of the electric field autocorrelation function. The three-time intensity correlation function is a six-time field correlation function that, if Gaussian, reduces to²⁴

$$g_G^{(3)}(\tau, \tau + T) = 1 + \beta[|\gamma(\tau)|^2 + |\gamma(T)|^2 + |\gamma(\tau + T)|^2] + 2\beta^2 \text{Re}[\gamma(\tau)\gamma(T)\gamma(\tau + T)]. \quad (8)$$

Similar predictions have appeared in prior literature,²⁷⁻²⁹ however none considered the nonzero detector area as accounted for here by factors of β .

For our measurements we employ two illumination and collection geometries: plane-in / plane-out equivalent,³⁰ and point-in / point-out. For both geometries, the sample is contained within a glass cell, and the incident beam is normal to the sample surface. Plane-in illumination is accomplished by expanding the laser beam with a diverging lens to be greater than the cell thickness. Point-in illumination is accomplished by passing the beam through a converging lens one focal length from the sample; the resulting spot size is about 0.5 mm. In all cases (including plane-equivalent³⁰), the detection spot size is slightly larger than the diameter of the GRIN lens, about 2 mm.

3. Diffusing particles

First we test our apparatus and procedures on diffusing Brownian particles. Our sample consists of polystyrene spheres, diameter $d = 93 \pm 8$ nm, suspended in a 53% glycerol

solution at a volume fraction of 1.86%, and contained in a 9 mm thick glass cell. This sample was previously measured at a slightly different wavelength.¹² At the wavelength used here, the average cosine of the scattering angle is $g = 0.102$ and the scattering mean free path is $l_s = 0.533$ mm; these give the transport mean free path $l^* = l_s/(1 - g) = 0.594$ mm. There is negligible absorption. The characteristic diffusion time that enters DWS predictions is $\tau_o = 1/(Dk^2) = 5.90$ ms, where D is the particle diffusion coefficient and k is wavenumber of the laser light in the solution.

Intensity autocorrelation results for a point-in / point-out backscattering geometry are shown in the top plot of Fig. 1. The separation distances between entry and collection spots, measured in units of l^* , for four different runs are $\rho = \{0, 1, 2, 4\}$. If the illumination and detection spots are small and if their separation is large, all in comparison with l^* , then the DWS prediction is $\gamma(\tau) = (1 + \rho\sqrt{6\tau/\tau_o}) \exp(-\rho\sqrt{6\tau/\tau_o})$.³¹ While these conditions do not hold for our experiments, we nevertheless find excellent fits to this form by adjusting the value of ρ . The resulting effective illumination-detection separation distances, in units of l^* , for our four runs are $\{1.8, 2.4, 4.1, 6.6\}$. To accurately model the intensity autocorrelation data, using the theory of DWS, would require knowledge of intensity and sensitivity vs position for the illumination and detection spots, respectively; however, this is not necessary for our main purpose of testing the validity of the Siegert relation.

Three-time intensity correlation results for point-in / point-out backscattering are shown in the bottom plot of Fig. 1. These data were collected simultaneously with the intensity autocorrelation data in the top plot, where the same constant delay time $T = 0.410$ ms was used for all four runs. To test whether the field statistics are Gaussian, we first extract the field autocorrelation assuming Eq. (2). Then we use it to generate the Gaussian expectation for $g^{(3)}(\tau, \tau + T)$ using Eq. (8). Finally we plot this expectation along with the actual data in Fig. 1b. Evidently, the Gaussian expectation agrees very well with the data. Therefore, we conclude, the electric field truly does have Gaussian statistics. This was expected, by design, because there are large numbers of uncorrelated diffusing particles within the scattering volume. This demonstration validates our experimental apparatus and methods. We now proceed to apply the same methods to a coarsening foam, which is not known in advance to be Gaussian.

4. Coarsening Foam

Our sample consists of Gillette Foamy shaving cream, composed by volume of 92% polydisperse gas bubbles tightly packed in an aqueous surfactant solution. With time, this foam coarsens due to the diffusion of gas from smaller to larger bubbles; drainage and film rupture are negligible. The sample container is a $L = 7$ mm thick glass cell with much larger lateral dimensions, so that light does not escape from the sides. All light scattering measure-

ments are performed after the foam has aged for 100 minutes in the sample cell. At this age, the average bubble diameter is $d = 60 \mu\text{m}$ and the photon transport mean free path is $l^* = 210 \mu\text{m}$.¹⁶ The measurement duration is 500 s, which is long enough to get a good measure of the intercept and baseline of the intensity autocorrelation, but small enough that the bubble size distribution does not significantly change.

The speckle pattern formed by scattered light fluctuates with time due to sudden structural rearrangements of small groups of neighboring bubbles from one packing configuration to another. These events relax local stress inhomogeneities that accumulate due to the coarsening process. The duration of a typical event is a few tenths of a second, while the time between successive events at any given location is roughly $\tau_o = 20$ s, for our 100 minute old samples. Thus, the bubbles are usually static and they rearrange only intermittently and quickly. Such dynamics are very different from thermal Brownian motion, where all particles gradually and independently move around. Therefore, for foam, the electric field statistics could conceivably be non-Gaussian either because most of the scattering sites are static, and hence correlated, or because the motion during an event is correlated throughout a scattering volume. Nevertheless, prior analysis has always assumed Gaussian field fluctuations that appear exactly like Brownian diffusion. The only difference is that now $\tau_o = 20$ s represents the time between rearrangement events at a given scattering site, as opposed to the time required for a particle to diffuse one wavelength.

Intensity autocorrelation results for a plane-in / plane-out transmission geometry are shown in the top plot of Fig. 2. At short times there is a slight gradual decay due to thermal motion of the bubble interfaces.¹⁸ At long times there is a full decay due to rearrangements that is well-described by $\gamma(\tau) = \sqrt{(L/l^*)^{26}\tau/\tau_o} / \sinh[\sqrt{(L/l^*)^{26}\tau/\tau_o}]$.¹⁶ Three-time intensity correlation data were acquired simultaneously for six different fixed delays, T , as labeled; the results are shown in the bottom plot of Fig. 2. The Gaussian expectation is generated directly from the intensity autocorrelation data, using Eqs. (2, 8), and the results are plotted along with the actual data Fig. 2b. Evidently the agreement is very good, justifying the long-standing assumption of Gaussian fluctuations for this geometry.

Next we carry out the same program for a plane-in / plane-out backscattering geometry. Since backscattering features shorter light paths than in transmission, there could now be non-Gaussian fluctuations. The results for the two- and three-time intensity correlations at six different fixed delay times, and the Gaussian expectation generated from the autocorrelation data, are all shown in Fig. 3. The field correlation function is well-described by $\gamma(\tau) = \exp(-2\sqrt{6\tau/\tau_o})$.¹⁶ The agreement between the Gaussian expectation and the actual three-time data is very good, again justifying the long-standing assumption of Gaussian fluctuations for this geometry.

Finally we repeat the same program for point-in / point-out backscattering geometries

with four different separation distances. The results for the two- and three-time intensity correlations at the same fixed delay time, and the Gaussian expectation generated from the autocorrelation data, are all shown in Fig. 4. By contrast with our other measurements, now we find non-Gaussian field fluctuations: the Gaussian expectation is systematically higher than the actual three-time intensity correlation data. Hence, the intensity autocorrelation is not described by the usual Siegert relation, Eq. (2), and the field correlation is not described by $\gamma(\tau) = (1 + \rho\sqrt{6\tau/\tau_0}) \exp(-\rho\sqrt{6\tau/\tau_0})$, as they were for the polyball sample of Fig. 1.

Because of the non-Gaussian character, there must be information available in the three-time intensity correlation that is not present in the intensity autocorrelation alone. But what information would this be? One possibility is fluctuations in the number of scattering sites within the scattering volume. There have been many demonstrations of how number fluctuations give rise to non-Gaussian effects.^{24,32,33} However, here we find Gaussian statistics for a polyball sample that has a larger l^* by a factor of two. Thus we believe that the extra information for a coarsening foam has to do with the intermittent nature of the rearrangement dynamics. One possibility is that the non-Gaussian character could be analyzed in terms of the rearrangement event size in comparison with the illumination / detection spot sizes. Another possibility is that it could be analyzed in terms of the switching functions that describe the statistics for how rearrangement events start and stop, as was done earlier for avalanches in intermittently-flowing sand.^{25,26} In either case, by contrast with number fluctuations, the non-Gaussian character is due to scattering site dynamics and is not evident in the intensity distribution. These possibilities could be investigated by multispeckle techniques such as TRC^{34,35} or SVS.^{36,37}

5. Conclusion

Higher-order temporal intensity correlation measurements are a powerful tool to confirm or deny the Gaussian character of electric field statistics. As applied to a coarsening foam, we find that prior assumptions of Gaussian fluctuations were indeed warranted; this was not obvious in advance. The only proviso is that the spot sizes in plane-in / plane-out equivalent geometries³⁰ be made sufficiently large in comparison with the rearrangement event size. The origin of non-Gaussian fluctuations for small spots sizes is likely due to the intermittent nature of the scattering site dynamics, by contrast with the well-known case of number fluctuations,^{24,32,33} and warrants further study.

Acknowledgments

We thank Pierre-Anthony Lemieux for technical assistance. This work was supported by NASA under Microgravity Fluid Physics Grant NAG3-2481.

References

1. J. H. Aubert, A. M. Kraynik, and P. B. Rand, "Aqueous foams", *Scientific American* **254**, 74-82 (1989).
2. J. Stavans, "The evolution of cellular structures", *Rep. Prog. Phys.* **56**, 733-89 (1993).
3. D. J. Durian and D. A. Weitz, "Foams," in *Kirk-Othmer Encyclopedia of Chemical Technology*, J. I. Kroschwitz, ed. (Wiley, New York, 1994), Vol. 11, pp. 783-805.
4. D. Weaire and S. Hutzler, "The Physics of Foams" (Clarendon Press, New York, 1999).
5. M. U. Vera, P.-A. Lemieux, and D. J. Durian, "Angular distribution of diffusely back-scattered light", *J. Opt. Soc. Am. A* **14**, 2800-8 (1997).
6. M. U. Vera, A. Saint-Jalmes, and D. J. Durian, "Scattering optics of foam", *Appl. Opt.* **40**, 4210-4 (2001).
7. A. S. Gittings, R. Bandyopadhyay, and D. J. Durian, "Photon channelling in foams", *Europhys. Lett.* **65**, 414-9 (2004).
8. M. Miri and H. Stark, "Persistent random walk in a honeycomb structure: Light transport in foams", *Phys. Rev. E* **68**, 031102/1-8 (2003).
9. M. F. Miri and H. Stark, "The role of liquid films for light transport in dry foams", *Europhys. Lett.* **65**, 567-73 (2004).
10. D. A. Weitz and D. J. Pine, "Diffusing-wave spectroscopy," in *Dynamic Light Scattering: The Method and Some Applications*, W. Brown, ed. (Clarendon, Oxford, 1993), pp. 652-720.
11. G. Maret, "Diffusing-wave spectroscopy", *Curr. Op. Coll. I. Sci.* **2**, 251-7 (1997).
12. P.-A. Lemieux, M. U. Vera, and D. J. Durian, "Diffusing-light spectroscopies beyond the diffusion limit: The role of ballistic transport and anisotropic scattering", *Phys. Rev. E* **57**, 4498-515 (1998).
13. B. J. Berne and R. Pecora, "Dynamic Light Scattering: With Applications to Chemistry, Biology, and Physics" (Dover Publications, New York, 2000).
14. B. Chu, "Laser Light Scattering, Basic Principles and Practice" (Academic Press, New York, 1991).
15. W. Brown, (Clarendon Press, Oxford, 1993), p. 0198539428.
16. D. J. Durian, D. A. Weitz, and D. J. Pine, "Multiple Light-Scattering Probes of Foam Structure and Dynamics", *Science* **252**, 686-8 (1991).
17. D. J. Durian, D. A. Weitz, and D. J. Pine, "Scaling Behavior in Shaving Cream", *Physical Review A* **44**, R7902-R5 (1991).
18. A. D. Gopal and D. J. Durian, "Fast thermal dynamics in aqueous foams", *J. Opt. Soc. Am. A* **14**, 150-5 (1997).
19. J. C. Earnshaw and A. H. Jaafar, "Diffusing-wave spectroscopy of a flowing foam", *Phys.*

- Rev. E **49**, 5408-11 (1994).
20. A. D. Gopal and D. J. Durian, "Nonlinear bubble dynamics in a slowly driven foam", Phys. Rev. Lett. **75**, 2610-3 (1995).
 21. S. Cohen-Addad and R. Hohler, "Bubble dynamics relaxation in aqueous foam probed by multispeckle diffusing-wave spectroscopy", Phys. Rev. Lett. **86**, 4700-3 (2001).
 22. P. Hebraud, F. Lequeux, J. P. Munch, and D. J. Pine, "Yielding and rearrangements in disordered emulsions", Phys. Rev. Lett. **78**, 4657-60 (1997).
 23. R. Hohler, S. Cohen-Addad, and H. Hoballah, "Periodic nonlinear bubble motion in aqueous foam under oscillating shear strain", Phys. Rev. Lett. **79**, 1154-7 (1997).
 24. P.-A. Lemieux and D. J. Durian, "Investigating non-Gaussian scattering processes by using nth-order intensity correlation functions", J. Opt. Soc. Am. A **16**, 1651-64 (1999).
 25. P.-A. Lemieux and D. J. Durian, "From avalanches to fluid flow: A continuous picture of grain dynamics down a heap", Phys. Rev. Lett. **85**, 4273-6 (2000).
 26. P.-A. Lemieux and D. J. Durian, "Quasi-elastic light scattering for intermittent dynamics", Appl. Opt. **40**, 3984-94 (2001).
 27. M. Corti and V. Degiorgio, "Intrinsic 3rd-order correlations in laser-light near threshold", Phys. Rev. A. **14**, 1475-8 (1976).
 28. G. D. J. Phillies, "Bispectral analysis as a probe of quasi-elastic light-scattering intensity fluctuations", J. Chem. Phys. **72**, 6123-33 (1980).
 29. L. Song and J. M. Schurr, "Three-Time Autocorrelation Function of the Power Associated with a Gaussian Random Process", Chem. Phys. **155**, 63-9 (1991).
 30. D. J. Durian, "Penetration Depth for Diffusing-Wave Spectroscopy", Appl. Opt. **34**, 7100-5 (1995).
 31. F. Morin, R. Borrega, M. Cloitre, and D. J. Durian, "Static and dynamic properties of highly turbid media determined by spatially resolved diffusive-wave spectroscopy", Appl. Opt. **41**, 7294-9 (2002).
 32. L. E. Estes, L. M. Narducci, and R. A. Tuft, "Scattering of light from a rotating ground glass", J. Opt. Soc. Am. **61**, 1301-6 (1971).
 33. P. N. Pusey, "Number fluctuations of interacting particles", J. Phys. A **12**, 1805-18 (1979).
 34. L. Cipelletti, H. Bissig, V. Trappe, P. Ballesta, and S. Mazoyer, "Time-resolved correlation: a new tool for studying temporally heterogeneous dynamics", J. Phys.-Cond. Matt. **15**, S257-S62 (2003).
 35. P. Mayer, H. Bissig, L. Berthier, L. Cipelletti, J. P. Garrahan, P. Sollich, and V. Trappe, "Heterogeneous dynamics of coarsening systems", Phys. Rev. Lett. **93**, 115701/1-4 (2004).
 36. P. K. Dixon and D. J. Durian, "Speckle visibility spectroscopy and variable granular

fluidization”, *Phys. Rev. Lett.* **90**, 184302/1-4 (2003).

37. R. Bandyopadhyay, A. S. Gittings, S. S. Suh, P. K. Dixon, and D. J. Durian, “Speckle-visibility spectroscopy: A tool to study time-varying dynamics”, *Rev. Sci. Inst.* **76**, 093110/1-11 (2005).

List of Figure Captions

Fig. 1. (color online) Two- and three-time intensity correlation functions for light backscattered from a colloidal suspension of polystyrene particles with a point-in / point-out geometry. Data are shown by symbols, while the Gaussian predictions based on autocorrelation data are shown by solid curves. The separation distance between the centers of the illumination and detection spots is given by ρ in units of the transport mean free path, l^* , as labeled. The fixed delay is $T = 0.410$ ms, as marked by an arrow.

Fig. 2. (color online) Two- and three-time intensity correlation functions for light transmitted through foam with a plane-in / plane-out equivalent geometry. Data are shown by symbols, while the Gaussian predictions based on autocorrelation data are shown by solid curves. The fixed delay time T is different for each of the six runs, as labeled.

Fig. 3. (color online) Two- and three-time intensity correlation functions for light backscattered from foam with a plane-in / plane-out equivalent geometry. Data are shown by symbols, while the Gaussian predictions based on autocorrelation data are shown by solid curves. The fixed delay time T is different for each of the six runs, as labeled.

Fig. 4. (color online) Two- and three-time intensity correlation functions for light backscattered from a foam with a point-in / point-out geometry. Data are shown by symbols, while the Gaussian predictions based on autocorrelation data are shown by solid curves. The separation distance between the centers of the illumination and detection spots is given by ρ in units of the transport mean free path, l^* , as labeled. The fixed delay is $T = 52.4$ ms, as marked by an arrow.

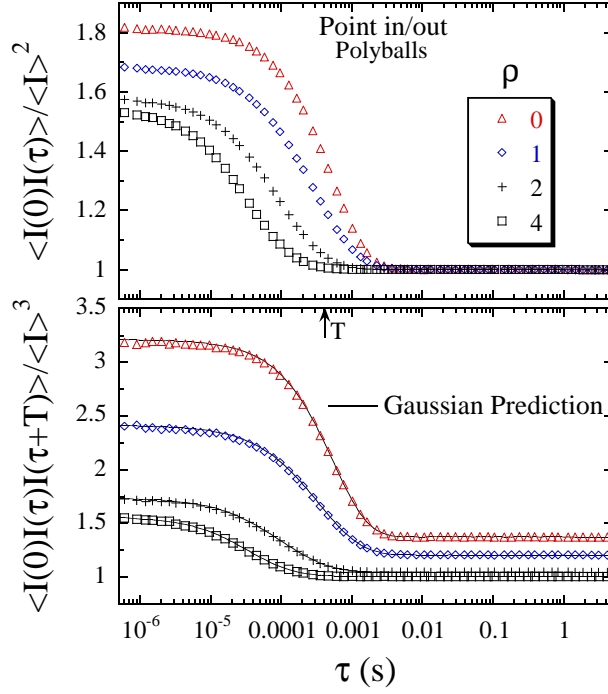


Fig. 1. (color online) Two- and three-time intensity correlation functions for light backscattered from a colloidal suspension of polystyrene particles with a point-in / point-out geometry. Data are shown by symbols, while the Gaussian predictions based on autocorrelation data are shown by solid curves. The separation distance between the centers of the illumination and detection spots is given by ρ in units of the transport mean free path, l^* , as labeled. The fixed delay is $T = 0.410$ ms, as marked by an arrow.

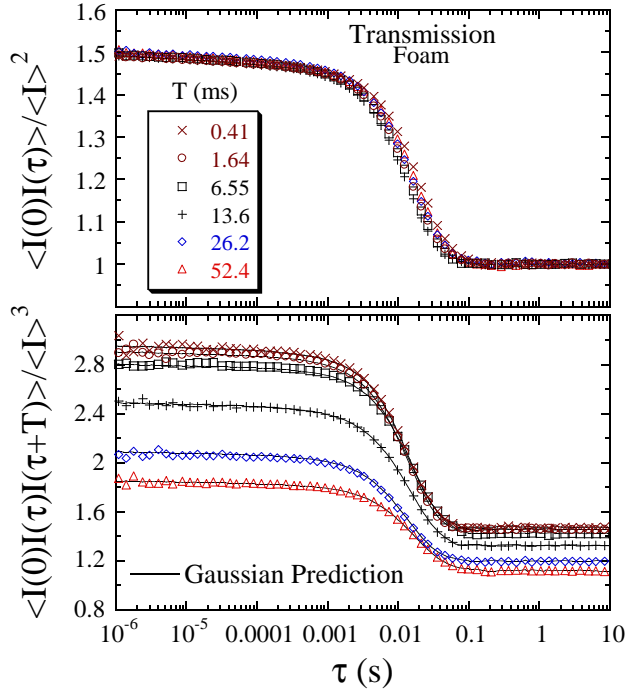


Fig. 2. (color online) Two- and three-time intensity correlation functions for light transmitted through foam with a plane-in / plane-out equivalent geometry. Data are shown by symbols, while the Gaussian predictions based on autocorrelation data are shown by solid curves. The fixed delay time T is different for each of the six runs, as labeled.

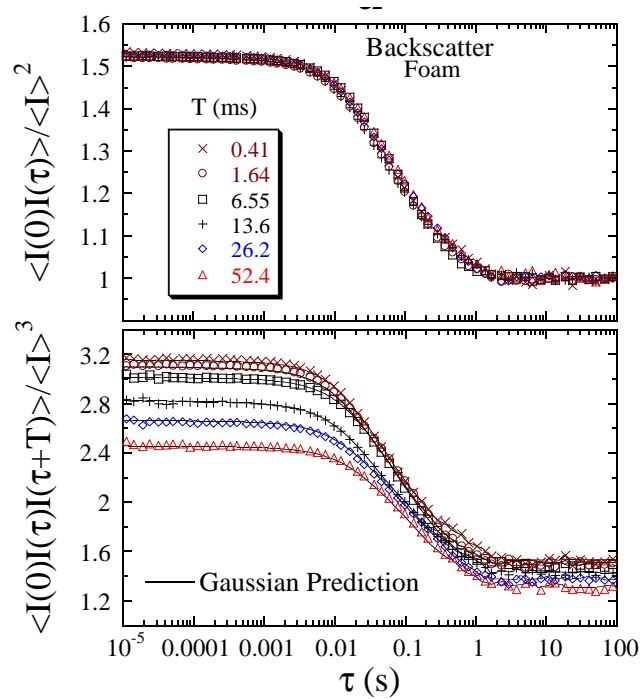


Fig. 3. (color online) Two- and three-time intensity correlation functions for light backscattered from foam with a plane-in / plane-out equivalent geometry. Data are shown by symbols, while the Gaussian predictions based on autocorrelation data are shown by solid curves. The fixed delay time T is different for each of the six runs, as labeled.

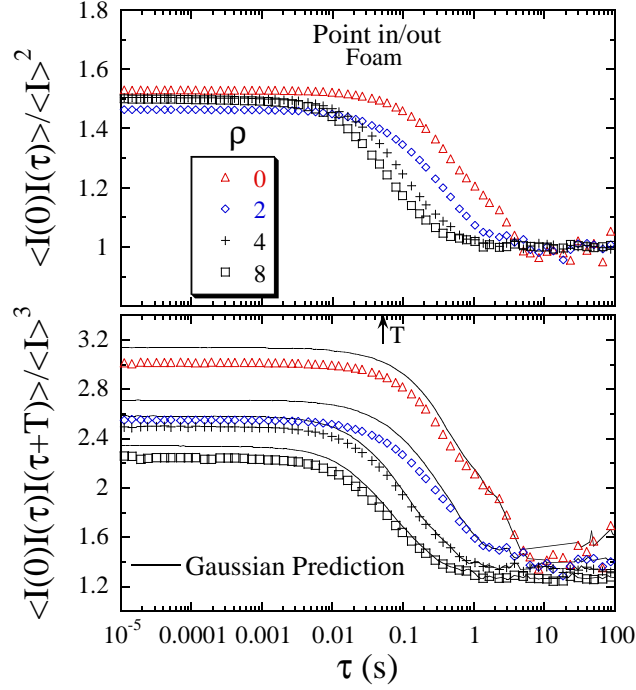


Fig. 4. (color online) Two- and three-time intensity correlation functions for light backscattered from a foam with a point-in / point-out geometry. Data are shown by symbols, while the Gaussian predictions based on autocorrelation data are shown by solid curves. The separation distance between the centers of the illumination and detection spots is given by ρ in units of the transport mean free path, l^* , as labeled. The fixed delay is $T = 52.4$ ms, as marked by an arrow.